

# 1 Marine snow latitudinal distribution in the equatorial Pacific along 2 180°

3 Gabriel Gorsky

4 Observatoire Océanologique, Laboratoire d'Océanographie de Villefranche-sur-Mer, CNRS/UPMC,  
5 Villefranche sur mer, France

6 Robert Le Borgne

7 Centre Institut de Recherche pour le Développement, Nouméa, New Caledonia

8 Marc Picheral and Lars Stemmann

9 Observatoire Océanologique, Laboratoire d'Océanographie de Villefranche-sur-Mer, CNRS/UPMC, Villefranche  
10 sur mer, France

11 Received 23 July 2001; revised 11 February 2003; accepted 7 March 2003; published XX Month 2003.

12 [1] Marine snow (MS) distribution from the surface to 1000 m depth was determined in  
13 the equatorial Pacific using the underwater video profiler during the Etude du Broutage en  
14 Zone Equatoriale cruise in fall 1996. The latitudinal transect was carried out at 17 stations  
15 along the 180° meridian from 8°S to 8°N during a cold phase of El Niño-Southern  
16 Oscillation. Higher MS concentrations were found below the equatorial zone than  
17 poleward. At the equator the estimated integrated MS carbon  $m^{-2}$  in the upper kilometer  
18 was  $5.7 g m^{-2}$ , while both southward and northward (between 1° and 8°) the mean  
19 integrated MS carbon was about  $2.7 g m^{-2}$ . In the upper 50 m the MS carbon was twofold  
20 lower than the combined carbon of autotrophic and heterotrophic protists and four times  
21 lower than the mesozooplankton carbon biomass, both measured concurrently during  
22 the cruise. Different water bodies had different MS content. The highest concentrations  
23 were found in the South Equatorial Current, the South Equatorial Counter Current, and the  
24 North Equatorial Countercurrent. Tropical waters at the south in the South Subsurface  
25 Countercurrents and the warm northern superficial waters had the lowest MS biomass.  
26 Mechanistically, a latitudinal “conveyor belt”, a poleward divergence of upwelled waters  
27 that return to the equator after being downwelled at north and south convergent zones,  
28 may partially explain the vertical distribution of particulate matter observed during the  
29 studied period. *INDEX TERMS*: 4805 Oceanography: Biological and Chemical: Biogeochemical cycles  
30 (1615); 4806 Oceanography: Biological and Chemical: Carbon cycling; 4283 Oceanography: General: Water  
31 masses; 4294 Oceanography: General: Instruments and techniques; 4863 Oceanography: Biological and  
32 Chemical: Sedimentation; *KEYWORDS*: equatorial Pacific, carbon cycling, particulate organic matter, marine  
snow, latitudinal advection, underwater video profiler

34 **Citation:** Gorsky, G., R. Le Borgne, M. Picheral, and L. Stemmann, Marine snow latitudinal distribution in the equatorial Pacific  
35 along 180°, *J. Geophys. Res.*, 108(C12), 8146, doi:10.1029/2001JC001064, 2003.

## 37 1. Introduction

38 [2] The equatorial Pacific is the main natural source of  
39 atmospheric CO<sub>2</sub> in the oceans [Tans *et al.*, 1990] but at the  
40 same time, it also acts as an important CO<sub>2</sub> sink because of  
41 its major contribution to global new production [Chavez  
42 and Barber, 1987; Chavez and Toggweiler, 1995]. Both  
43 new production and CO<sub>2</sub> evolution mechanisms are closely  
44 linked to equatorial upwelling, which varies temporally and  
45 spatially. To the west is the warm pool region, characterized  
46 by an oligotrophic stratified structure. The zonal boundary  
47 between oligotrophic and upwelling regions is influenced  
48 by interannual variations associated with the El Niño-  
49 Southern Oscillation (ENSO) cycle [Picaut *et al.*, 1996;

*Le Borgne et al.*, 2003]. On shorter timescales, community 50  
structure, functioning of the upwelling ecosystem and thus 51  
the downward export of the upper layer primary productiv- 52  
ity respond to seasonal cycles, equatorial Kelvin waves and 53  
tropical instability waves [Dunne *et al.*, 2000, Eldin and 54  
Rodier, 2003; Le Borgne *et al.*, 2003]. 55

[3] Particles are responsible for the vertical transport of 56  
material in the ocean. Marine snow particles (i.e., macro- 57  
scopic marine aggregates >500  $\mu m$ ) are ubiquitous and may 58  
dominate the total mass sinking flux because of their 59  
abundance and rapid settling rates [Asper, 1987]. Ranging 60  
from pure phytoplankton flocks to amorphous detritus and 61  
zooplankton remains [Allredge and Silver, 1988], particles 62  
are of different sizes and origins and subjected to different 63  
kinds and degrees of water column processing. Their sinking 64  
trajectories and dissolution/aggregation processes are there- 65

fore difficult to interpret. Nonetheless, *Walsh and Gardner* [1992] demonstrated that sediment trap estimates of carbon fluxes in the equatorial Pacific were proportional to the concentration and size distribution of large aggregates.

[4] Phytoplankton biomass in the equatorial Pacific upwelling zone is characterized by latitudinal gradients with the highest values being generally observed at or near the equator [*Chavez, 1989, Brown et al., 2003; Le Bouteiller et al., 2003*]. The fate of the phytoplankton in this region is an important issue with respect to the importance of the biological pump. According to *Dam et al.* [1995] and *Gaudy et al.* [2003], a large proportion of the carbon ingested by mesozooplankton is not phytoplankton. Most of the direct grazing of primary producers is done by microzooplankton [*Landry et al., 1995; Le Borgne and Landry, 2003*]. Organic aggregates form as the result of grazing and detrital processes acting on the phytoplankton. While rapidly sinking dense fecal pellets can be quantified from sediment traps [*Fowler and Knauer, 1986*], this is not the case for the porous, marine snow like particles (MS). Direct in situ measurements of the standing stocks of MS particles are difficult because of their fragile nature, but *Allredge* [1998] has shown that particle mass is a function of size and that elemental compositions are similar regardless of origin, composition or season of collection. Imaging methods therefore provide an alternative in situ approach to quantifying the abundances and distribution patterns of undisturbed large particles. Although several still and video camera systems have been developed for this purpose [*Honjo et al., 1984; Asper, 1987; Gardner and Walsh, 1990; MacIntyre et al., 1995; Walsh et al., 1997; Gorsky et al., 1992, 2000*], studies applying these imaging approaches across system gradients in the oceans are still relatively few.

[5] The French Etude du Broutage en Zone Equatoriale (EBENE) cruise, conducted during a cold ENSO period in 1996 in the framework of the international JGOFS program, provided an opportunity to study large particulate matter as part of a broad investigation of food web interactions in the equatorial Pacific upwelling region. In this paper, we report on the latitudinal distribution of MS in the first kilometer of the equatorial Pacific along the 180° meridian from 8°S to 8°N.

## 2. Materials and Methods

[6] Data on the vertical distribution of particulate matter (>460 μm) were collected with the underwater video profiler (UVP) [*Gorsky et al., 1992, 2000, 2002*] during the French EBENE cruise (23 October to 12 November 1996) onboard R/V *L'Atalante*. The cruise consisted of a sampling transect along the 180° dateline, with stations being made at every degree of latitude between 8°N and 8°S.

### 2.1. Underwater Video Profiler

[7] The UVP (model #3), developed at the Observatoire Oceanographique de Villefranche sur mer, France is a multi-array instrument composed of the following sensors: Exavision XC 644 black and white video camera equipped with a 12 mm focal distance lens, a Sony video recorder, a fluorometer and a nephelometer (both Chelsea Instruments Ltd.) coupled to a Seabird 19 CTD probe. Particles contained in a known volume of water (1.3 l), are illuminated by two

54 W Chatwick Helmut stroboscopes delivering a collimated light beam. Environmental data gathered by the other sensors is recorded simultaneously. The system is independently powered by 24V batteries and is controlled by a Texas 370 microprocessor. A complete 0–1000 m vertical profile with the UVP system consists of approximately 25,000 images, taken at a 1m s<sup>-1</sup> lowering speed and an acquisition rate of 25 images s<sup>-1</sup> (<http://www.metal-process.com>).

### 2.2. Data Analysis

[8] Data are processed by two custom-built programs. The first one, written in Visual C++ (Microsoft), digitizes the images without compression and performs the image analysis, saving the number of particles per image and their attributes to an ASCII file. The second program (MATLAB, Scientific Software) is used for data processing and editing. Particles are enumerated and their individual cross-sectional areas, lengths and Equivalent Spherical Diameters (ESD) determined. Particle volumes are obtained from ESDs, and the individual aggregate volumes are converted into carbon biomass estimates using the dry weight (DW) to aggregate size relationship of *Allredge and Gotchalk* [1989] and the C:DW ratio of 0.2 found for large refractory aggregates [*Allredge, 1998*].

[9] Particle abundances and size spectra are averaged, respectively, for 5 and 20-m thick layers. The metric surface (Y) as a function of the pixel surface (X) can be expressed by the following equations obtained from laboratory calibrations [see *Gorsky et al., 2000*]:

$$12 \text{ mm} : Y = 0.02 X^{1.137}, \quad R^2 = 0.873$$

[10] Data processing only applies to the portion of the vertical profile where images display a constant dark background since sunlight interferes with the collimated light beam. Therefore the analysis starts at depth where such interference becomes negligible. This was not a problem for most of the station profiles, which were sampled at night. However, sunlight effects limited the analyses to depths below 90 m at 4°S and 5°N, below 25 m at 2°S, and below 110 m at 7°S and 2°N. Because of a power failure, data at 8°S were acquired only from the surface to 160 m.

[11] With the exception of the missing depth ranges given above, MS size distributions were averaged for 6 depth strata (0–50, 50–125, 125–250, 250–500, 500–750, and 750–1000 m) at each of the 17 transect stations. The hierarchical flexible clustering was performed on a matrix of Kolmogorov distances among these size distributions [*Legendre and Legendre, 1984*]. At a distance of 45, three types of size distributions could be discriminated. This distance can be used for the detection of variation between distributions. Thus the distributions of the “large particles” group is characterized by higher frequency of particles >0.5 mm, compared to the other two distributions. Particles <0.5 mm dominate the group of “small particles” [see *Stemann et al., 2000*].

## 3. Results

### 3.1. Water Circulation and Marine Snow Distributions

[12] As described by *Eldin and Rodier* [2003], the South Equatorial Current (SEC) was flowing westward at 180°, between 5°S and 4°N, during the EBENE cruise, and the

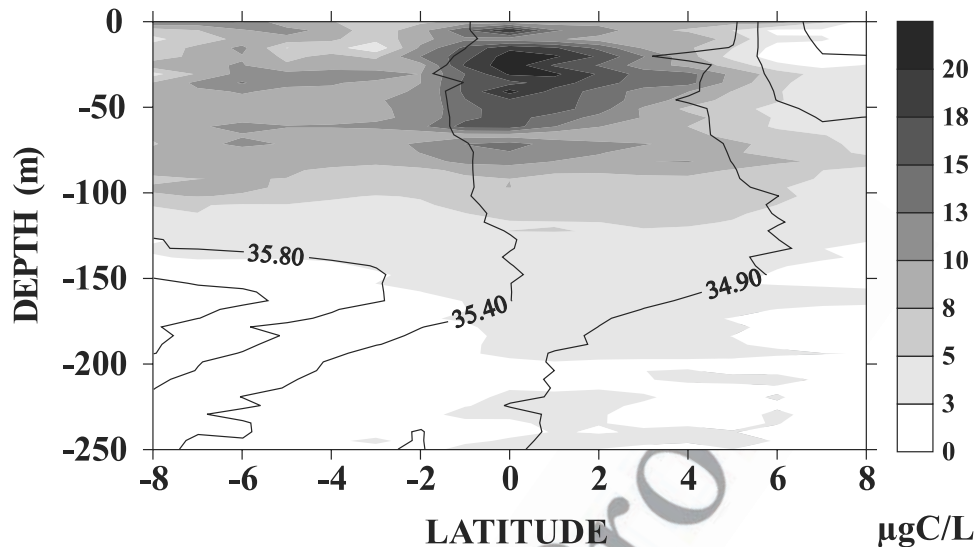


**Figure 1.** Latitudinal distributions of marine snow carbon mass (gray scale) and the salinity field (psu) in the upper 250 m of the EBENE equatorial transect.

185 North Equatorial Countercurrent (NECC) flowed eastward,  
 186 north of 4°N. Subsurface flow consisted of the eastward  
 187 flowing Equatorial Under-Current (EUC), centered at the  
 188 equator below 100 m. The South and North Subsurface  
 189 Countercurrents (SSCC, NSCC) also flowed eastward  
 190 below 200 m south of 6°S and north of 2°N, respectively.  
 191 The maximum velocity of the SEC was 90 cm/s (north of  
 192 the equator), while the highest velocity of the EUC was  
 193 60 cm/s. The Equatorial Intermediate Current (EIC) flowed  
 194 westward below the EUC between 0° and 2°N. The South  
 195 Equatorial Counter Current (SECC) was observed south of  
 196 5°S and was associated with the deepening of the warm  
 197 surface waters [Eldin and Rodier, 2003]. A tongue of high-  
 198 salinity and particle-depleted tropical water (TW) was  
 199 present in the thermocline, south of 1°S (Figure 1).

200 [13] Isotherm gradients were influenced by the geostrophic  
 201 zonal circulation. Near the surface, temperature values were

lowest at the equator and highest on both ends of the  
 202 latitudinal transect. At the equator, the 28°C isotherm that  
 203 defines the top of the upper thermocline extended almost to  
 204 the surface because of upwelling. Both turbidity and fluores-  
 205 cence values were highest in the equatorial zone. Fluores-  
 206 cence maxima deepened poleward, from 50 m at the equator  
 207 to about 80 m at 8°S and below 100 m at 8°N (data not  
 208 shown). MS concentrations peaked near the equator at the  
 209 surface and also in the underlying deep layers (Figure 2).

210 [14] MS concentrations are compared in Table 1 for the  
 211 different water types, selected according to the flow fields  
 212 described by Eldin and Rodier [2003]. MS concentrations  
 213 were high in the lower part of the SECC, above the TW.  
 214 Particulate densities were very low in the saline TW, and  
 215 remained so in the SSCC. Subsurface minimum concen-  
 216 trations of MS were observed in the EUC, whereas the  
 217 highest midwater values, exceeding one third of surface  
 218

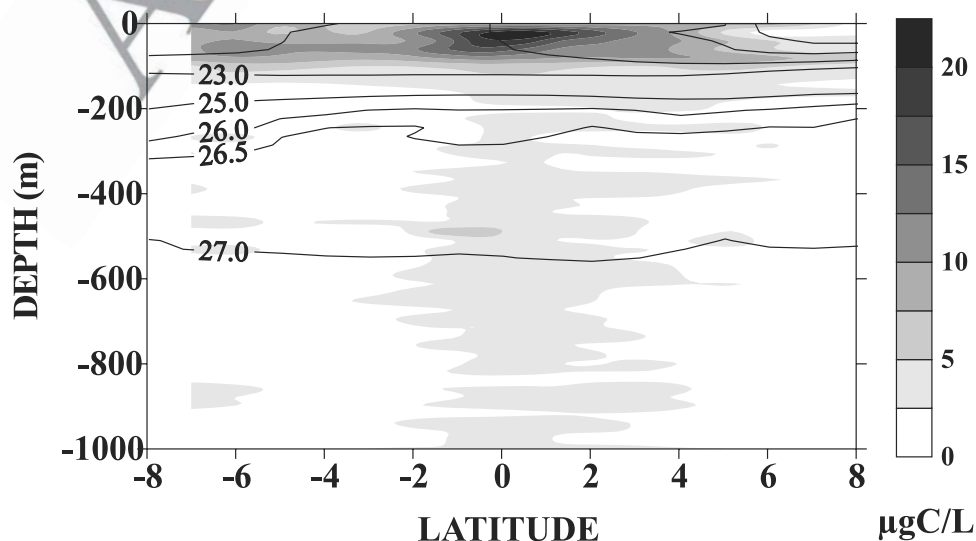


**Figure 2.** Vertical distributions of >460- $\mu\text{m}$  marine snow particles ( $\mu\text{g C L}^{-1}$ ) in relation to the 0–100 m density field ( $\sigma\text{-}\theta$ ) along the EBENE equatorial transect. Data below 160 m are missing at 8°S.

t1.1 **Table 1.** Mean Concentrations, Volumes (ppm), and Carbon Weights ( $\mu\text{g L}^{-1}$ ) of Marine Snow (MS) Particles in Different Water

	7°S,		6°S,		3°S,		0°		1°N,		1°N,		3°N,		6°N,		8°N,	
	SECC	S.D.	TW	S.D.	SSCC	S.D.	EUC	S.D.	Upper	Lower	SEC	S.D.	NSCC	S.D.	NECC	S.D.	Oligo	S.D.
t1.3	110–150		160–200		250–300		150–200		0–100		250–300		200–300		50–150		0–50	
t1.4	4.11	1.65	0.62	0.33	1.24	0.51	3.10	0.93	9.95	5.77	3.25	1.07	2.74	0.94	3.28	1.84	1.68	0.99
t1.5	0.91	0.22	0.11	0.10	0.16	0.11	1.15	1.48	2.35	2.42	0.62	0.27	0.58	0.38	0.53	0.34	0.44	0.36
t1.6	4.72	1.64	0.68	0.39	1.20	0.58	3.71	1.50	11.32	6.98	3.65	1.29	3.07	1.07	3.47	1.98	2.05	1.27

t1.7 <sup>a</sup>SECC, South Equatorial Counter Current (data above 110 m were not available); TW, Tropical Waters; SSCC, South Subsurface Counter Current; EUC, Equatorial Undercurrent; EIC, Equatorial Intermediate Current; SEC, South Equatorial Current; NSCC, North Subsurface Counter Current; ECC, North Equatorial Counter Current; Oligo, warm northern surface waters (stations 6°N, 7°N and 8°N); and S.D., standard deviation. For detailed descriptions of the hydrological conditions, see *Eldin and Rodier* [2003].

219 values, were measured in the EIC around 300 m. MS  
 220 concentrations were similar in the NSCC and the EUC.  
 221 Warm surface waters north of 6°N displayed lower concen-  
 222 trations of particles than deeper in the NECC. Overall,  
 223 equatorial stations had higher concentrations of large par-  
 224 ticles (size distributions were determined using the hierar-  
 225 chical flexible clustering method [see *Stemmann et al.*,  
 226 2000]). Large aggregates were observed at the station 6°S  
 227 and in the superficial oligotrophic waters of the stations 7°N  
 228 and 8°N, but in low numbers (1–2 aggregates 1–1).  
 229 Elsewhere, the smaller MS size classes prevailed. In sub-  
 230 surface layers, MS concentrations were high in the equato-  
 231 rial zone and in the SECC and NECC.

232 [15] Comparison of MS concentrations in different layers  
 233 against the mean value calculated for the whole transect  
 234 shows that only the equatorial MS values were consistently  
 235 higher in concentrations and volume than the latitudinal  
 236 mean. All values obtained at stations 5°S and 7°N were  
 237 lower than the latitudinal mean. At 6°S, the concentration  
 238 and volume were higher than the mean in the upper 150 m,  
 239 but not in below. Globally, the stations south of the equator  
 240 (5°–2°S) displayed a deficit when compared to the MS  
 241 latitudinal mean. Northern stations (1°–3°N) had MS con-  
 242 centrations higher than the mean (Figure 3). Station 4°N  
 243 separated the near equatorial stations with higher MS  
 244 concentration from peripheral stations with low superficial  
 245 concentration. The convergence zone between 4 and 5°N  
 246 was also the site of accumulation and downward export of  
 247 the autotrophic and heterotrophic microbial biomass [*Brown*  
 248 *et al.*, 2003].

249 [16] Four main hydrographic patterns can be discerned  
 250 when T/S profiles of the sampled stations are compared (not  
 251 shown here) [*Eldin and Rodier*, 2003]. One characterizes  
 252 stations south of the equator, the second is the equatorial  
 253 station, the third includes northern stations near the equator,  
 254 and the three extreme northern stations comprise the fourth.  
 255 Examining the distributions of particulate carbon from the  
 256 surface to 1000 m along the cross-equatorial transect, it  
 257 appears that the relatively high values are grouped in a  
 258 narrow temperature and salinity range. Concentrations  
 259 exceeding  $15 \mu\text{g C L}^{-1}$  were found in the surface layer at  
 260 only three stations (1°S, 0° and 1°N), and the highest MS  
 261 concentrations were distributed along a salinity gradient  
 262 extending from 35 to 35.5 (Figure 4). Station 6°S showed  
 263 high MS concentrations only in the upper 150 m. Beneath  
 264 this depth, in the high-salinity tropical water (TW), the  
 265 particle load was much lower, and the resulting integrated

MS carbon was equivalent to the corresponding northern 266  
 stations. 267

### 3.2. Latitudinal Size Distribution 268

[17] Generally, decreases in MS particle abundances are 269  
 coupled with the increasing individual particle size 270  
 [Stemmann *et al.*, 2000]. In the present study, large particles 271  
 were found in the upper 250 m, mostly between 2°S and 272  
 4°N (Figure 5). Abundance distributions were often nega- 273  
 tively correlated with the size at individual stations (c.f. 274  
 stations 7° and 8°N). However, around the equator (from 275  
 1°S to 1°N), the abundance of large particles was high in the 276  
 superficial layers. 277

## 4. Discussion 279

### 4.1. MS Depth Distributions 280

[18] Interactions between the different water masses may 281  
 influence the fate of surface produced biogenic matter. 282  
 Diatoms, for instance, have the potential to form flocs that 283  
 sink eventually to deeper layers [*Allredge and Gotschalk*, 284  
 1989; *Kiorboe et al.*, 1998]. During the EBENE cruise, 285  
*Brown et al.* [2003] observed the highest accumulation of 286  
 large diatoms in surface waters near the equator. The 287  
 abundance of large particles measured by the UVP was 288  
 also highest in the equatorial surface layer (Figure 5). Our 289  
 results show, however, that the MS concentration decreased 290  
 in the EUC, forming a discontinuity between the near- 291  
 surface and deep layers. Such a discontinuity and the low 292  
 zooplankton biomass below 100 m [*Le Borgne et al.*, 2003], 293  
 raise the following question: what processes influence the 294  
 vertical distribution of marine snow? 295

[19] *Walsh et al.* [1997] proposed a conceptual model in 296  
 which the equatorial upwelling results in a poleward diver- 297  
 gent flow of near-surface waters. Following a circular 298  
 pattern, surface flow reaches northern and southern conver- 299  
 gence zones and returns to the equator in the deeper layers. 300  
 The effects of frontal subduction are difficult to measure 301  
 directly but may be suggested by the spatial distribution of 302  
 chlorophyll pigments [*Kadko et al.*, 1991; *Send et al.*, 1999; 303  
*Videau et al.*, 1994] or by the vertical distribution of large 304  
 particulates. For instance, *Gorsky et al.* [2002] found that 305  
 fast sinking particles, such as large aggregates, sediment 306  
 near the site of their production, while small and porous 307  
 aggregates can be advected substantial distances before they 308  
 sink. 309

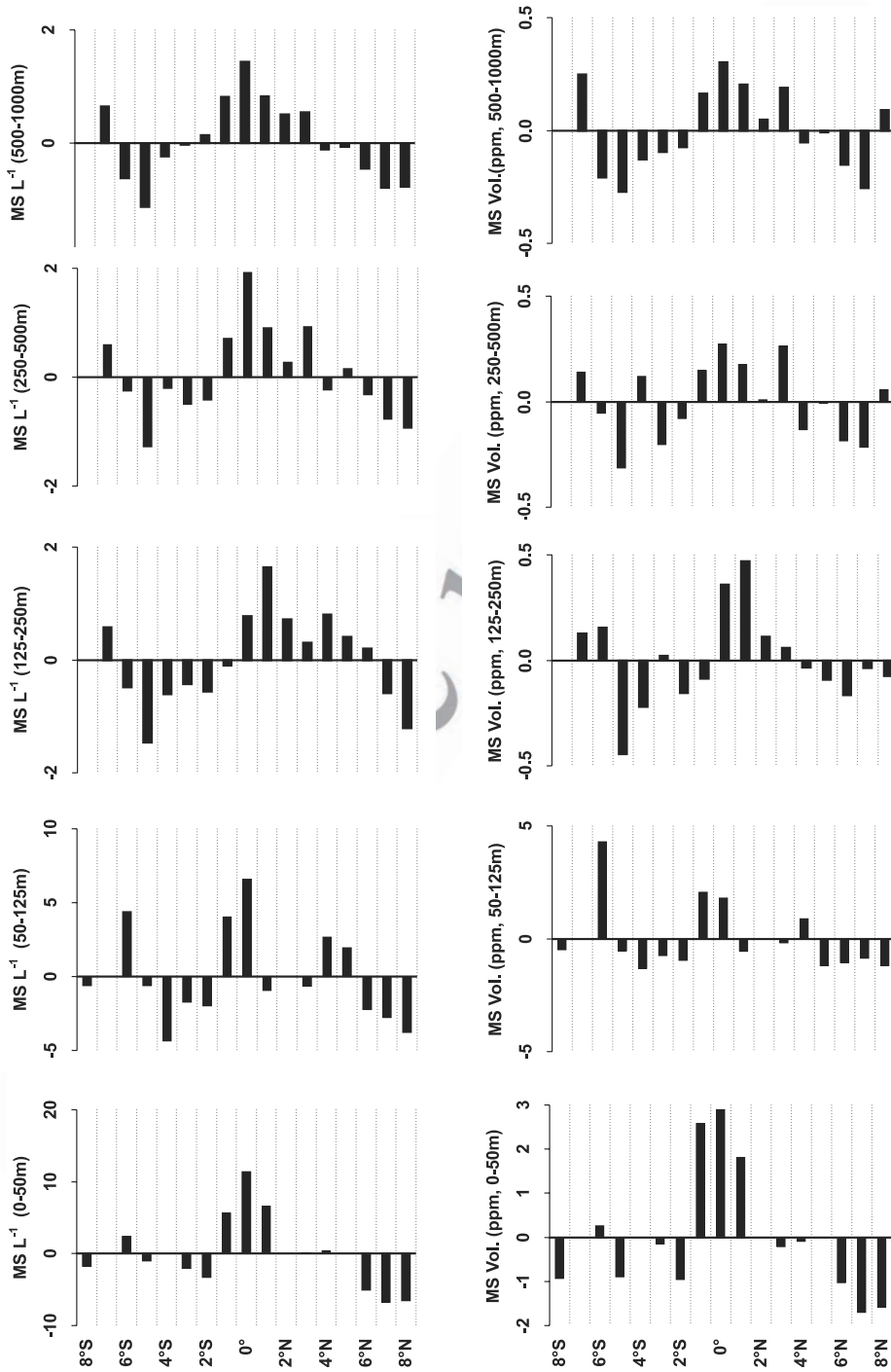


**Figure 3.** Variability of marine snow (MS) concentrations in different depth strata around the latitudinal mean ( $\equiv 0$ ) for EBENE equatorial transect.

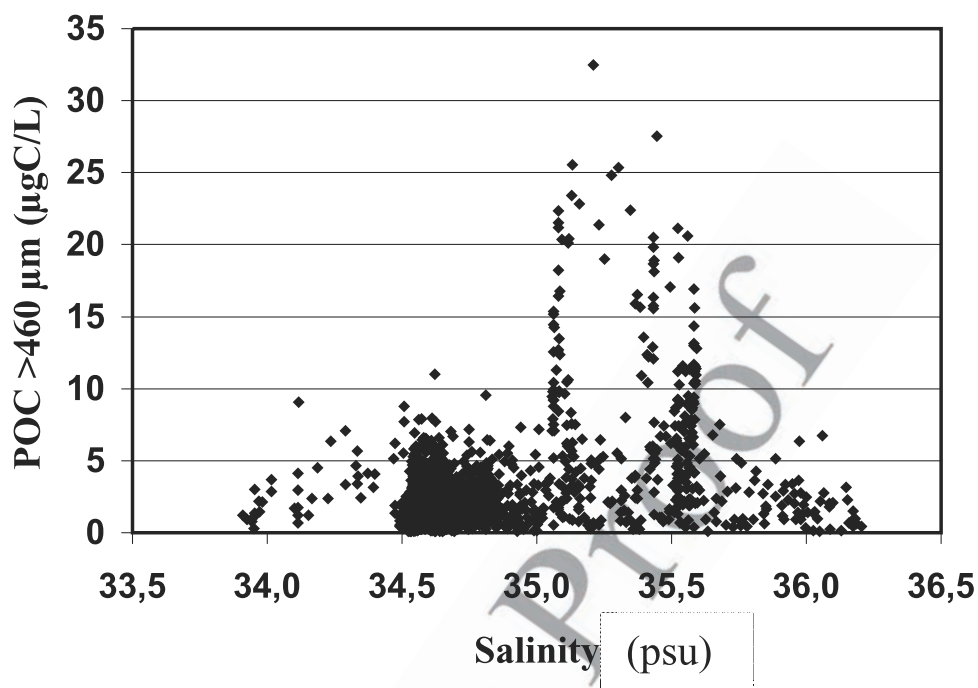


**Figure 4.** Carbon biomass of marine snow (MS) particles, as estimated by the underwater video profiler, as a function of salinity along the EBENE latitudinal section.

310 [20] Two convergence zones are evident in the current  
 311 profiles of the EBENE equatorial cross section provided by  
 312 *Eldin and Rodier* [2003]. One is in the vicinity of 4°N, where  
 313 *Eldin and Rodier* [2003] found an anomalous deepening of  
 314 the surface layer corresponding to a horizontal convergence  
 315 between a strong NECC north of 4°–5°N and the SEC  
 316 (westward flow between 5°S and 4°N). A second conver-  
 317 gence appears at 5°S between the SEC and the SECC. The  
 318 two convergences, marked by a deepening of the thermo-  
 319 cline at 4°N and 5°S, may induce an advective transport of  
 320 organic matter. The meridional surface flows are the results  
 321 of upwelling and poleward divergence occurring between  
 322 the EUC and SEC [*Walsh et al.*, 1997]. This surface flow is  
 323 mixed and downwelled at convergence zones and returns as  
 324 a subsurface return flow to the equator. Mechanistically, this  
 325 subsurface return flow could act as a latitudinal conveyor

belt, transporting part of the advected surface biological  
 production back to deeper equatorial layers.

326  
 327  
 328 [21] According to *MacIntyre et al.* [1995], turbulence  
 329 may contribute to the accumulation of small particles. In  
 330 fall 1996, biological production peaked at the equator.  
 331 *Brown et al.* [2003] studied the abundance and composition  
 332 of the microbial community on the EBENE equatorial cross  
 333 section. The accumulation of photosynthetic and heterotro-  
 334 phic biomass observed by the latter authors between 4° and  
 335 5°N could fuel the particle aggregation processes during the  
 336 downwelling of water masses at the convergent fronts.  
 337 Large aggregates could then be produced continuously  
 338 during the advective transport back to the equatorial zone.  
 339 Such a mechanism may explain the observed discontinuity  
 340 in MS concentrations between the superficial and deeper  
 341 equatorial layers (Figure 2) and the observed change in MS

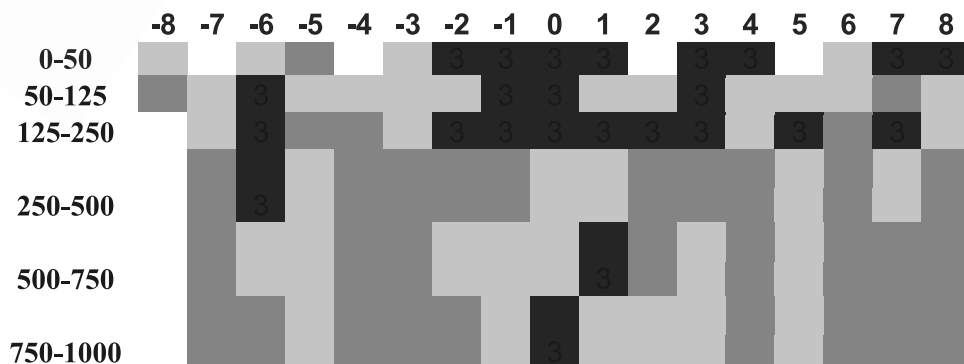


**Figure 5.** Latitudinal section of the relative proportions of large, medium, and small marine snow particles in different depth strata along the EBENE transect. Black rectangles, large particles; dark gray rectangles, medium-sized particles; light gray rectangles, the smallest size class particles; and white rectangles, missing data.

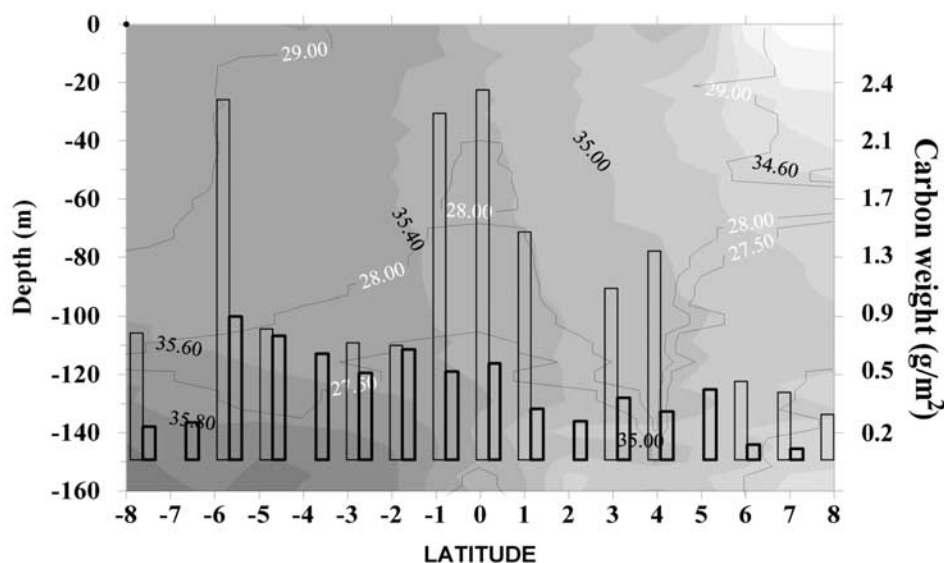


**Figure 6.** Depth-integrated (0–150 m) carbon estimates of marine snow particles (histograms) relative to surface temperature (isolines with white labels) and salinity (contour plot, dark labels) fields along the EBENE transect.

vertical distribution at 4°N (Figure 3). On the other hand, the high concentration of MS in the upper 150 m at 6°S could be associated both with the frontal feature between the SEC and the SECC (Figure 6) and with the horizontal intrusion of the TW below 150 m limiting the vertical dilution of particles. Although weaker during the EBENE cruise, the southern convergence has been previously described as an active feature [Radenac and Rodier, 1996].

#### 4.2. MS as a Carbon Reservoir

[22] MS carbon content was calculated for each individual particle detected optically using the relationships of Alldredge and Gotschalk [1988] and Alldredge [1998]. Results obtained by different imaging systems under similar conditions are comparable [MacIntyre *et al.*, 1995; Jackson *et al.*, 1997]. Our results show that MS standing stock averaged  $2.7 \text{ g C m}^{-2}$  in the upper kilometer of the water column in the southern part of the transect,  $5.6 \text{ g C m}^{-2}$  at the equator and  $2.7 \text{ g C m}^{-2}$  at the northern stations (Table 2). MS concentrations peaked in surface waters near the equator and also in the underlying deep layers (Figure 2). In the upper 50 m, the combined average autotrophic and heterotrophic carbon biomass associated with  $<200\text{-}\mu\text{m}$  protists was about twofold higher than the MS carbon mass and about four times higher than mesozooplankton carbon [Brown *et al.*, 2003; Le Borgne *et al.*, 2003].

[23] Diel vertical migration of mesozooplankton (200–2000  $\mu\text{m}$ ) was investigated during the two long-term stations, the equator and 3°S, during the EBENE cruise [Le Borgne *et al.*, 2003]. Over the 0–400 m depth range, day/night differences in mesozooplankton biomass were not significant. In the equatorial HNLC zone, mesozooplankton were concentrated in the superficial 100 m layer and consisted mainly of surface living, nonmigratory species [Le Borgne *et al.*, 2003]. Although the carbon content of the heterotrophic microbial community below 100 m was not measured, the decrease of the autotrophic particles and

zooplankton carbon mass with depth emphasizes the importance of the MS as particulate carbon pool in the ocean’s interior (Table 2).

[24] As a consequence of the surface distribution and reduced diel migrations of mesozooplankton in the HNLC water column, the “active” export of carbon from the euphotic zone is relatively low. Therefore the latitudinal “conveyor belt” as proposed by Walsh *et al.* [1997] may play a nonnegligible role in the vertical flux of organic matter to deeper equatorial layers. Because of the complex climatic forcing and zonal water circulation more data are necessary to support the proposed circulation mechanism for MS particles.

#### 5. Conclusions

[25] As for most biological parameters, the equatorial upwelling zone is marked by a near-surface biomass maximum in marine snow particles. However, because of the strong shear between the SEC and the EUC and to the upwelling divergence, there is a discontinuity between MS

**Table 2.** Mean Integrated Carbon Weight (in  $\text{mg C m}^{-2}$ ) of Marine Snow (MS) Particles in the Southern, Equatorial, and Northern Stations of the Latitudinal Transect for Each Depth Layer<sup>a</sup>

Depth, m	South	S.D.	0°	North	S.D.
50–0	595	482	1157	431	319
100–50	443	242	875	298	158
150–100	167	74	288	178	98
200–150	68	23	192	139	65
400–200	317	107	700	428	149
1000–400	1117	840	2464	1244	913
Total 0–1000	2707		5676	2718	

<sup>a</sup>S.D. is standard deviation. MS carbon values (in  $\text{mg C m}^{-2}$ ) are calculated from equivalent spherical diameters following Alldredge and Gotschalk [1989] and Alldredge [1998].

t2.1  
t2.2  
t2.3  
t2.4  
t2.5  
t2.6  
t2.7  
t2.8  
t2.9  
t2.10

concentrations in the surface and deep waters. Our hypothesis for such a discontinuity is that part of the equatorial surface MS, as well as other biogenic matter that ultimately aggregates into large particulates, is transported poleward to the southern and northern convergence zones, where it sinks and is transported back to the equator by deep currents. If this mechanism is correct, it provides another example of the importance of latitudinal effects on production processes in the equatorial Pacific. In other words, in this dynamic system which experiences a strong zonal advection, slow latitudinal transport cannot be neglected when considering the fate of primary production.

[26] The significant standing stocks of marine snow with respect to phytoplankton biomass may be explained by different turnover times of these two particulate pools. While phytoplankton biomass turns over rapidly, the slower formation and decay processes of amorphous particles allows the accumulation of substantial mass. This may also indicate that the consumption of marine snow is rather low.

[27] **Acknowledgments.** We thank M. R. Landry and M. Youngbluth for helpful comments, the crew of R/V *Atalante* from IFREMER for the efficient technical assistance and the IRD, INSU-CNRS and the EURAPP EC program under contract MAS-CT98-061 for financial support.

## References

- Aldredge, A. L., The carbon, nitrogen and mass content of marine snow as function of aggregate size, *Deep Sea Res., Part I*, 45, 529–541, 1998.
- Aldredge, A. L., and C. C. Gotschalk, In situ settling behavior of marine snow, *Limnol. Oceanogr.*, 33, 339–351, 1988.
- Aldredge, A. L., and C. C. Gotschalk, Direct observations of the flocculation of diatom blooms: Characteristics, settling velocity and formation of diatom aggregates, *Deep Sea Res., Part A*, 36, 159–171, 1989.
- Aldredge, A. L., and M. W. Silver, Characteristics, dynamics and significance of marine snow, *Prog. Oceanogr.*, 20, 41–82, 1988.
- Asper, V. L., Measuring the flux and sinking speed of marine snow aggregates, *Deep Sea Res., Part A*, 34, 1–17, 1987.
- Brown, S., M. R. Landry, J. Neveux, and C. Dupouy, Microbial community abundance and biomass along a 180° transect in the equatorial Pacific during an ENSO cold phase, *J. Geophys. Res.*, 108(C12), 8139, doi:10.1029/2001JC000817, in press, 2003.
- Chavez, F. P., Size distribution of phytoplankton in the central and eastern tropical Pacific, *Global Biogeochem. Cycles*, 3, 27–35, 1989.
- Chavez, F. P., and R. T. Barber, An estimate of new production in the equatorial Pacific upwelling, *Deep Sea Res., Part A*, 34, 1229–1243, 1987.
- Chavez, F. P., and J. R. Toggweiler, Physical estimates of global new production: The upwelling contribution, in *Upwelling in the Ocean: Modern Processes and Ancient Records*, edited by C. P. Summerhayes et al., pp. 313–320, John Wiley, Hoboken, N. J., 1995.
- Dam, H. G., X. Zhang, M. Butler, and M. R. Roman, Mesozooplankton grazing and metabolism at the equator in the central Pacific: Implications for carbon and nitrogen fluxes, *Deep Sea Res., Part II*, 42, 735–755, 1995.
- Dunne, J. P., J. W. Murray, M. Rodier, and D. A. Hansell, Export flux in the western and central equatorial Pacific: Zonal and temporal variability, *Deep Sea Res., Part I*, 47, 901–936, 2000.
- Eldin, G., and M. Rodier, Ocean physics and nutrient fields along 180° during an ENSO cold phase, *J. Geophys. Res.*, 108(C12), 8137, doi:10.1029/2000JC000746, in press, 2003.
- Fowler, S., and G. A. Knauer, Role of large particles in the transport of elements and organic compounds through the oceanic water column, *Prog. Oceanogr.*, 16, 147–194, 1986.
- Gardner, W. D., and I. D. Walsh, Distribution of macroaggregates and fine-grained particles across a continental margin and their potential role in fluxes, *Deep Sea Res., Part A*, 37, 401–411, 1990.
- Gaudy, R., G. Champalbert, and R. Le Borgne, Feeding the metabolism of mesozooplankton in the equatorial Pacific HNLC zone: Consequences on the particulate biomass, *J. Geophys. Res.*, 108(C12), 8144, doi:10.1029/2000JC000743, in press, 2003.
- Gorsky, G., C. Aldorf, M. Kage, M. Picheral, Y. Garcia, and J. Favole, Vertical distribution of suspended aggregates determined by a new underwater video profiler, *Ann. Inst. Oceanogr.*, 68, 13–23, 1992.
- Gorsky, G., M. Picheral, and L. Stemmann, Use of the underwater video profiler for the study of aggregate dynamics in the north Mediterranean, *Estuarine Coastal Shelf Sci.*, 50, 121–128, 2000.
- Gorsky, G., L. Prieur, I. Taupier-Letage, L. Stemmann, and M. Picheral, Large particulate matter (LPM) in the western Mediterranean. I - LPM distribution related to hydrodynamics, *J. Mar. Syst.*, 33–34, 289–311, 2002.
- Honjo, S. K., K. W. Doherty, Y. C. Agrawal, and V. L. Asper, Direct optical assessment of large amorphous aggregates (marine snow) in the deep ocean, *Deep Sea Res., Part A*, 31, 67–76, 1984.
- Jackson, G. A., R. Maffione, D. K. Costello, A. L. Alldredge, B. Logan, and H. G. Dam, Particle size spectra between 1 μm and 1 cm at Monterey Bay determined using multiple instruments, *Deep Sea Res., Part I*, 44, 1739–1767, 1997.
- Kadko, D. C., L. Washburn, and B. Jones, Evidence of subduction within cold filaments of the northern California coastal transition zone, *J. Geophys. Res.*, 96, 14,909–14,926, 1991.
- Kiorboe, T., P. Tiselius, B. Mitchell-Innes, J. L. S. Hansen, A. W. Visser, and X. Mari, Intensive aggregate formation with low vertical flux during an upwelling-induced diatom bloom, *Limnol. Oceanogr.*, 43, 104–116, 1998.
- Landry, M. R., J. Constantinou, and J. Kirshtein, Microzooplankton grazing in the central equatorial Pacific during February and August, 1992, *Deep Sea Res., Part II*, 42, 657–671, 1995.
- Le Borgne, R., and M. R. Landry, EBENE: A JGOFS investigation of plankton variability and trophic interactions in the equatorial Pacific (180°), *J. Geophys. Res.*, 108(C12), 8136, doi:10.1029/2001JC001252, in press, 2003.
- Le Borgne, R., G. Champalbert, and R. Gaudy, Mesozooplankton biomass and composition in the equatorial Pacific along 180°, *J. Geophys. Res.*, 108(C12), 8143, doi:10.1029/2000JC000745, 2003.
- Le Bouteiller, A., J. Blanchot, and J. Neveux, Primary production, new production, and growth rate in the equatorial Pacific: Changes from mesotrophic to oligotrophic regime, *J. Geophys. Res.*, 108(C12), 8141, doi:10.1029/2000JC000914, in press, 2003.
- Legendre, L., and P. Legendre, *Ecologie*, vol. 1, *Le Traitement Multiple des Données Écologiques*, Coll. Ecol., vol. 1, 260 pp., Masson, Québec, Canada, 1984.
- MacIntyre, S., A. L. Alldredge, and C. C. Gotschalk, Accumulation of marine snow at density discontinuities, *Limnol. Oceanogr.*, 40, 449–468, 1995.
- Picaut, J., M. Ioualalen, C. Menkes, T. Delcroix, and M. J. McPhadden, Mechanism of the zonal displacement of the Pacific warm pool: Implication for ENSO, *Science*, 274, 1486–1489, 1996.
- Radenac, M.-H., and M. Rodier, Nitrate and chlorophyll distributions in relation to thermohaline and current structures in the western tropical Pacific during 1985–1989, *Deep Sea Res., Part II*, 43, 725–752, 1996.
- Send, U., J. Font, G. Krahnmann, C. Millot, M. Rhein, and J. Tintore, Recent advances in observing the physical oceanography of the western Mediterranean Sea, *Prog. Oceanogr.*, 44, 37–64, 1999.
- Stemmann, L., M. Picheral, and G. Gorsky, Diel variation in the vertical distribution of particulate matter (>0.15 mm) in the NW Mediterranean Sea investigated with the underwater video profiler, *Deep Sea Res., Part I*, 47, 507–534, 2000.
- Tans, P. P., I. Y. Fung, and T. Takahashi, Observational constraints on the global atmospheric CO<sub>2</sub> budget, *Science*, 247, 1431–1438, 1990.
- Videau, C., A. Sournia, L. Prieur, and M. Fiala, Phytoplankton and primary production characteristics at selected sites in the geostrophic Almeria-Oran front system (SW Mediterranean Sea), *J. Mar. Syst.*, 5, 235–250, 1994.
- Walsh, I. D., and W. D. Gardner, A comparison of aggregates profiles with sediment trap fluxes, *Deep Sea Res., Part A*, 39, 1817–1834, 1992.
- Walsh, I. D., W. D. Gardner, M. J. Richardson, S. P. Chung, C. A. Plattner, and V. L. Asper, Particle dynamics as controlled by the flow field of the eastern equatorial Pacific, *Deep Sea Res., Part II*, 44, 2025–2047, 1997.
- G. Gorsky, M. Picheral, and L. Stemmann, Observatoire Océanologique, LOV, CNRS/UPMC, BP 28, 06230 Villefranche sur mer, France. (gorsky@obs-vlfr.fr; picheral@obs-vlfr.fr)
- R. Le Borgne, Centre IRD, B.P. A5, Nouméa Cédex, New Caledonia.